The Institution of Engineering and Technology

RPG 2022
Renewable Power Generation

22-23 September 2022

Meeting net zero carbon

Savoy Place, London

Call for papers deadline:
10 December 2021

#RPGLondon

Received: 30 September 2020 | Revised: 20 May 2021 | Accepted: 24 May 2021

DOI: 10.1049/rpg2.12225

IET Renewable Power Generation

The Institution of Engineering and Technology WILEY

ORIGINAL RESEARCH PAPER

A novel doubly-fed doubly-salient machine with DC-saturation-relieving structure for wind power generation

Jifu Jiang | **Xiaodong Zhang** | **Shuangxia Niu** | **Xing Zhao**

Department of Electrical Engineering, Hong Kong Polytechnic University, Hung Hom, Hong Kong

Correspondence
Shuangxia Niu, Department of Electrical Engineering, Hong Kong Polytechnic University, Hung Hom, Hong Kong
Email: eesxniu@polyu.edu.hk

Funding information
National Natural Science Foundation of China, Grant/Award Number: 52077187; Research Grant Council of the Hong Kong Government, Grant/Award Numbers: PolyU 152143/18E, PolyU 152109/20E

Abstract

This paper presents a novel doubly-fed doubly-salient machine (DF-DSM) with DC-saturation-relieving effect for wind power generation application, which possesses the advantages of enhanced torque density, reduced torque ripple and improved power density. The key is that PMs are introduced into the stator slot openings to mitigate the saturation effect in stator core caused by DC field excitation, and relatively large excitation current can be fed into stator field windings, which contributes to improved power density of machine. In addition, with the armature winding artificially connected, the reluctance of all magnetic paths is kept the same, and the variation of self-inductance is compensated, and the torque ripple is greatly suppressed. In this paper, the machine structure and DC-saturation-relieving working principle are introduced. The slot-pole combinations are analysed, and dimension parameters are optimized. By using time-stepping finite-element analysis, the electromagnetic performance of optimal machine is evaluated which verifies the validity of the proposed design.

1 | INTRODUCTION

With the development of industries, environmental pollution and energy shortage have become two main problems around the world. Recently, wind power generation has attracted more and more attention due to its non-polluting and renewable characteristics [1–4]. Wind power generator is the core component of the wind power generation system. Nowadays, most of yearly installed turbines are variable speed wind turbines [5, 6]. Variable speed wind turbines enable the wind power generator to realize the maximum power absorption over a wide range of wind speeds.

Permanent magnet doubly-salient machine (PMDSM), combining the structure of switching reluctance machine and PM material, has been widely accepted for wind power applications with its inherent high efficiency, high power density as well as robust structure [7–12]. However, due to the fixed excitation from PMs, it is not easy for the PMDSM to offer controllable air-gap flux and extend the speed range to capture more wind energy. Recently, many efforts have been made to solve this problem. In PMDSM, the DC field winding could be used to replace the PMs, and the doubly fed doubly salient machine (DF-DSM) can realize flexible flux control [13–15]. However, due to the mutual magnetic path is shared with armature winding and field windings, saturation effect in stator core under the overload conditions will unavoidably affect the wind energy harvesting and power production of machine. Lots of efforts have made to solve stator core saturation problems to improve the power conversion of machine [16–24].

In order to solve aforementioned problems, a novel DF-DSM with DC-saturation-relieving effect is proposed in this paper, which not only provides excellent flexible flux control with DC field excitation, but also enhances the power density with tangentially magnetized PMs mounted in the slot opening. In addition, with special design of the magnetic paths and winding connections, relatively small self-inductance variation and torque ripple can be achieved.

In Section 2, the machine configuration and DC-saturation-relieving principle are illustrated in detail. In Section 3, slot-pole combination is analysed and machine dimension parameters are

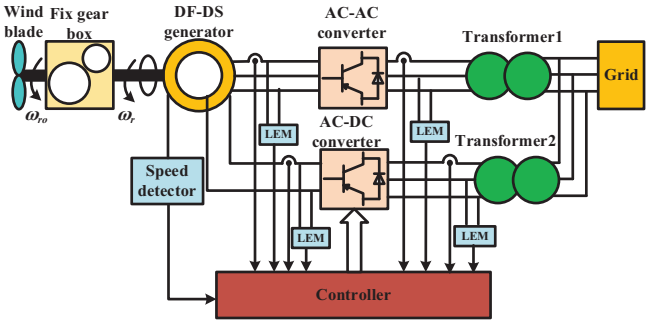

FIGURE 1 System configuration

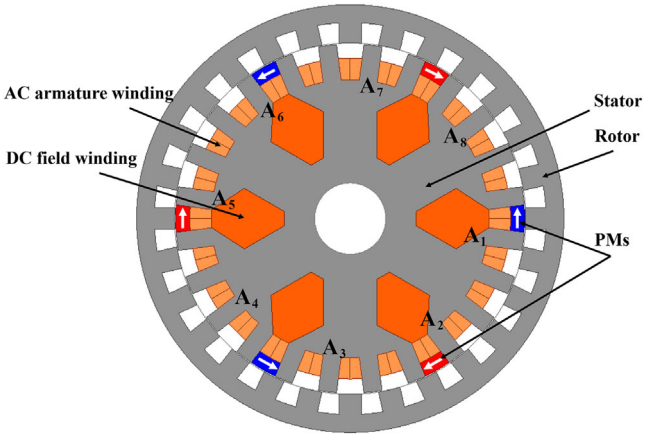

FIGURE 2 Structure of proposed machine

optimized. In Section 4, the electromagnetic performance of the proposed machine is investigated by finite-element analysis (FEA). In Section 5, the conclusions are drawn from the investigation.

2 | MACHINE STRUCTURE AND WORKING PRINCIPLE

2.1 | System configuration and machine structure

The configuration of the wind power system is denoted in Figure 1. It is mainly composed of wind blade for wind power capture, fixed gear to step up the wind speed for high-speed operation, and a three-phase DF-DSM for the electromechanical energy conversion. The AC armature winding of the machine is connected to AC–AC converter and then transformer 1, providing electricity for power grid, while the DC field winding is connected to an AC–DC converter and is supplied with the electricity coming from power grid. Voltage signals, current signals, as well as speed signals are transferred to the controller, and then the controller gives the switching signal to the AC–AC converter and AC–DC converter. Therefore, with changeable DC field excitation variable speed constant voltage wind power generation can be realized.

Figure 2 shows the structure of proposed DF-DSM with DC-saturation-relieving structure. The machine is composed of a 24-slot stator and a 28-pole rotor, with a doubly salient structure. Since the rotor consists of only iron core, the machine is provided with good mechanical robustness. The stator has all excitation sources, namely, slot PMs, DC field winding, and AC armature winding is also located in stator side. While the DC field winding uses a single-layer concentrated connection, the AC armature winding adopts a double-layer concentrated connection as showed in Figure 3. In the machine, slot PMs are artificially introduced to mitigate DC saturation of the stator core caused by DC field excitation. All slot PMs are magnetized in tangential direction.

The merits of proposed DF-DSM with DC-saturation-relieving structure are listed as following.

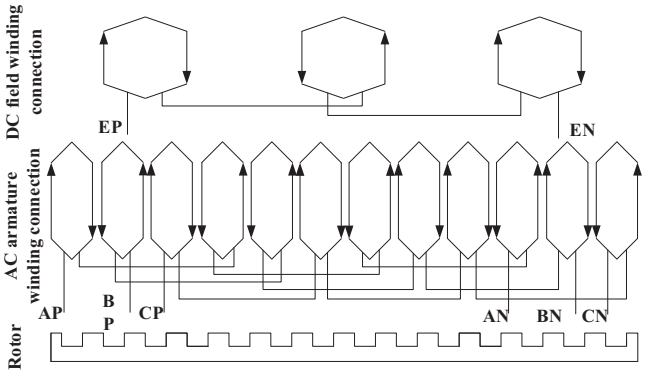

FIGURE 3 Winding connection of proposed machine

1. The rotor is composed of only iron core, which provides a good mechanical robustness.
2. Tangentially magnetized PMs are inset into the slot opening, which can greatly reduce the DC saturation of the stator core caused by DC field excitation so as to improve the torque density of machine.
3. With the DC-field saturation relieving design, increased DC field excitation current can be flexibly controlled, which offers enhanced power production over a wide wind speed range and increases wind energy conversion.
4. With special selection of stator pole number, the rotor pole number, the DC field excitation pole number, as well as the phase number, the doubly salient machine can realize three phase symmetry of the flux linkage and back EMF, insignificant variation of the self-inductance, as well as reduced torque ripple.

2.2 | DC-saturation-relieving principle

Figure 4 denotes the no-load flux distribution under different excitation sources, using 1/2 machine model. When only DC current is applied as shown in Figure 4(a), the flux linkage excited by DC current is an independent magnetic circuit unit.

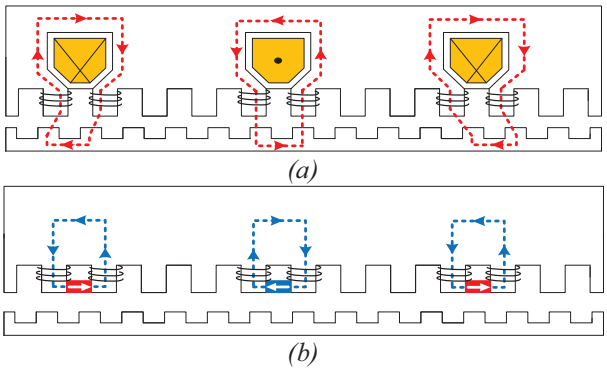

FIGURE 4 No-load flux distribution of 1/2 model. (a) Only idc. (b) Only slot PMs

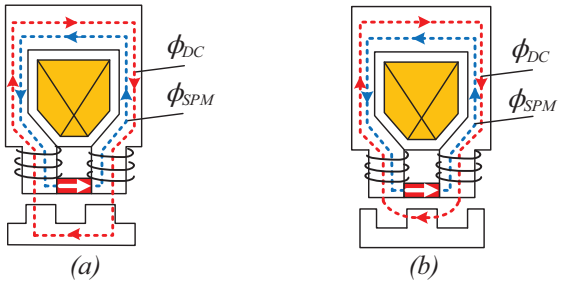

FIGURE 5 No-load flux distribution with both idc and slot PMs

When only slot PMs are used as shown in Figure 4(b), the flux linkage direction excited by slot PMs is opposite to that excited by DC current.

Figure 5 presents the no-load flux distribution with both dc current and PM excitations when rotor position varies in DF-DSM with DC-saturation-relieving structure. As shown in Figure 5(a), when the rotor salient pole is aligned with stator tooth, the DC field excitation loop reluctance is minimized. In this way, the DC field coil flux attains the maximum value. On the contrary, as denotes in Figure 5(b), when the rotor salient pole is unaligned with stator tooth, the DC field excitation loop reluctance is maximized. In this way, the DC field coil flux reaches the minimum value. DC field coil flux is biased and has large DC component, which makes stator core easily saturated. However, tangentially magnetized PMs are mounted on the slot opening, which can efficiently mitigate the DC saturation of the stator core caused by DC field excitation. Due to the minimum reluctance principle, slots PMs flux links the stator core all the time, which would not be affected by the rotor position. It can be seen in Figure 5, since the constant slot PM flux direction is opposite to the DC field flux direction, the stator DC saturation can be reduced to enhance back-EMF and steady torque.

Figure 6 gives the no-load flux variation with different rotor position. When the rotor salient pole is aligned with stator tooth, it is called aligned position. When the rotor salient pole is unaligned with stator tooth, it is called unaligned position. The *d* axis is corresponding to aligned position, and q axis is corresponding to medium position, between aligned position and unaligned position. As shown in Figure 6(a), with only DC field

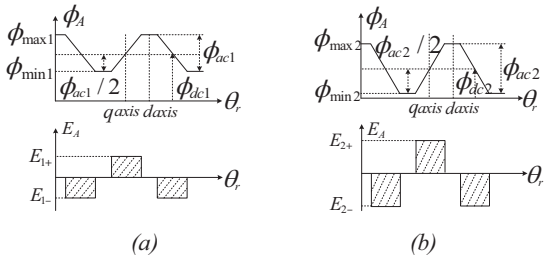

FIGURE 6 No-load flux variation and back-EMF with different rotor position. (a) Only idc with DC saturation. (b) Both idc and slot PMs with relieved DC saturation

excitation, the flux is biased and has large dc component ϕ_{dc1}. In this case, the stator core is saturated, DC field flux maximum value ϕ_{max1} is limited by stator core saturation. As shown in Figure 6(b), with introducing of slot PMs, the dc component excited by dc field current is reduced to ϕ_{dc2}. Since DC saturation of stator core are significantly relieved, DC field flux maximum value ϕ_{max2} is no longer limited by stator core saturation. In this case, the AC component ϕ_{ac2} is definitely larger than AC component ϕ_{ac1}, which leads to larger back-EMF and torque.

3 | MACHINE DESIGN OPTIMIZATION

3.1 | Slot-pole combination

In this paper, an analytical and FEA combined method is applied to find out the optimal slot-pole combination. For conventional DSMs, the relationship between the number of stator poles N_s, the number of rotor poles N_r, the number of DC field excitation poles N_{dc}, as well as the number of phases m are not purposely selected. Therefore, the conventional DSMs exist several shortcomings as following:

1. Because of different relative positions of phase windings to the DC field coils, magnetic circuits of all phases are asymmetrical. The flux passing through the coil on the middle tooth is less than flux passing through the coil wound on the tooth near DC field winding slots. Therefore, the back EMF waveform of each phase is not identical.
2. When salient pole of rotor is aligned with the stator tooth, the flux linkage of each AC armature coil reaches the maximum value. In contrast, when salient pole of rotor is unaligned with the stator tooth, the flux linkage of each AC armature coil attains the minimum value. The variation of flux linkages near two position are different because of the stator iron saturation. Therefore, the left and right sides of the EMF waveform are asymmetric and current will be deformed.
3. For the existing DSMs, the self-inductance of each AC armature coil varies simultaneously with rotor movement and each AC armature coil has the same pattern of variation of self-inductance. Because of the series connection of AC armature coils per phase, the resulting variation of

TABLE 1 Fundamental data of the proposed machine

Rated voltage	V	110
Rated torque	Nm	50
Rated speed	rpm	600
Number of turns per AC armature coil	/	40
Number of turns per DCfield coil	/	10
PM remanence	T	1.1
PM coercivity	kA/m	838
Steel saturated flux density	T	1.8
Steel mass density	kg/m	7820

self-induction per phase is actually an integer multiple of the variation of each AC armature coil. Therefore, the variation of self-inductance per phase is large, which would lead to large torque ripple.

In order to solve above mentioned problems, two criteria are proposed. First, every phase composes of coils distributed in all locations relative to each DC field excitation pole. Therefore, the number of phase coils under a DC field excitation pole should be different from the number of phases. The first criterion can be donated as:

$$(m + k)\ N_{dc} = N_s\ =\ mk_1 \tag{1}$$

where k and k_1 are positive integers and $k < m$.

Second, the stator slot pitch should be equal to the angular difference of two adjacent phases, which can be expressed according to number of rotor poles and the number of stator poles. The second criterion can be expressed as:

$$360°k_2 \pm \alpha\ =\ 360°\frac{N_r}{N_s} \tag{2}$$

where, k_2 is positive integer and α is slot pitch. For example, when $m = 3$ and $N_{dc} = 6$ is given, $N_r = 20/28$ and $N_s = 24$ can be deduced from Equations (1) and (2).

Therefore, FEA models with 24/20 and 24/28 slot-pole combinations are compared. Fundamental data of proposed machine is given in Table 1. Dimension parameters are depicted in Figure 7 and initial values of dimension parameters are shown in Table 2.

Considering the slot-pole combination is counted as the most leading design parameter, a simplified comparison is adopted in this process, which greatly saves optimization time. All the models share the same design parameters apart from the rotor pole number as well rotor tooth width. Besides, DC field excitation is the main source for torque generation. Hence, only DC field excitation without slot PMs is regard as the criterion for comparison. In this case, slot PMs is removed.

With FEA analysis, the steady torque with 24/20 and 24/28 slot-pole combinations are shown in Figure 8. It can be seen that, comparing with 24/20 case with 16.46 Nm rated torque, 24/28 case has much higher rated torque namely about 34.34 Nm. Torque ripple ratio of 24/20 case is 0.45, while that of 24/28 case is 0.32. Therefore, the 24/28 case is used for further analysis.

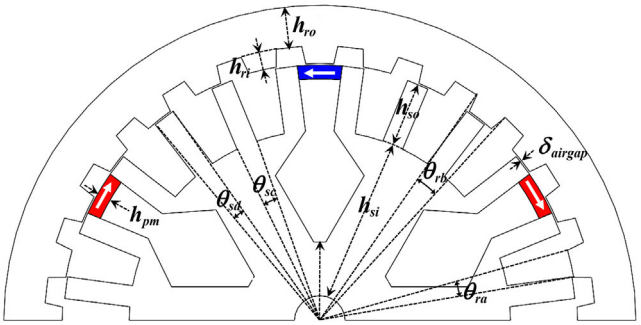

FIGURE 7 Dimension parameters of proposed machine

TABLE 2 Initial dimension parameters of proposed machine

Symbol	Parameter	Unit	Value
R_{ro}	Outer radius of rotor	mm	120
R_{si}	Inner radius of stator	mm	97
h_{ro}	Height of rotor yoke	mm	16
h_{ri}	Height of rotor slot	mm	7
h_{so}	Height of stator slot	mm	16
h_{si}	Height of stator yoke	mm	60
l	Stack length	mm	80
δ_{airgap}	Airgap length	mm	0.6
h_{pm}	Height of slot-PMs	mm	4
θ_{ra}	Arc of rotor tooth top	rad	0.010
θ_{rb}	Arc of rotor tooth bottom	rad	0.122
θ_{sc}	Arc of stator tooth bottom	rad	0.106
θ_{sd}	Arc of stator tooth top	rad	0.080

3.2 | Machine parameter optimization

Once the slot-pole combination is determined, other dimension parameters should be further optimized to boost machine

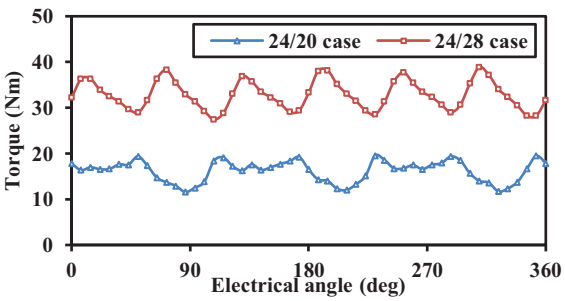

FIGURE 8 Torque under different slot-pole combinations

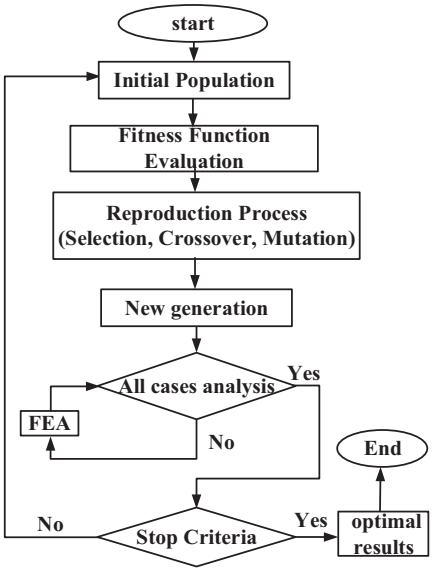

FIGURE 9 Flowchart of the GA and FEA coupled optimization

TABLE 3 GA Parameters

Parameter	Value
Population size	50
Number of generations	20
Probability of crossover	0.6
Probability of mutation	0.04

electromagnetic performance. However, it is difficult to optimized machine dimension parameters by traditional analytical method owning to the complexity of magnetic field distribution. An intelligent algorithm, namely, genetic algorithm (GA) is used and communicates with Maxwell to achieve combined optimization [17]. GA is a biologically inspired searching and optimizing algorithm, which can generate high quality results relying on the computer technology. GA has three significant operators, namely, selection, crossover as well as mutation, the same as the process of nature selection.

The flowchart of the GA and maxwell coupled optimization is presented in Figure 9 and the GA parameters are shown in Table 3. In this paper, the maximum torque density and minimum torque ripple are taken as two optimization objectives. The initial population are produced randomly, and then they are evaluated by fitness function (muti-objective function). Relatively high-quality ones have more opportunities to be selected, and then go through crossover and mutation. Therefore, a new generation is born. All cases in the new generation should analysed by FEA. Several stop criteria determine whether the loop stop or not. If it is satisfied, we get final population and optimal results.

The optimal results of each case in the last generation are shown in Figure 10. It can be noticed that some cases have relatively lower average torque and lower torque ripple, while some cases have relatively higher average torque and higher torque ripple. However, it exists some cases have relatively higher aver-

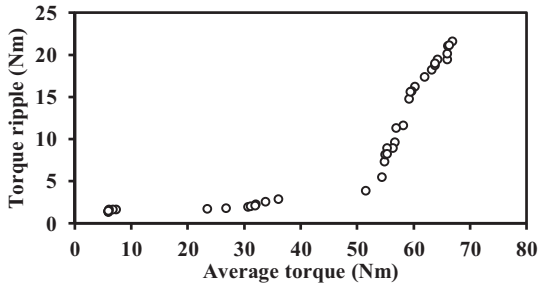

FIGURE 10 Optimal cases in the last generation

TABLE 4 Dimensions of the proposed machine

Parameter	Lower limit	Upper limit	Initial value	Optimal value
h_{ro}(mm)	8	22	16	15.46
h_{ri}(mm)	5	15	7	6.74
θ_{ra}(rad)	0.08	0.16	0.1000	0.1086
θ_{rb}(rad)	0.10	0.18	0.1220	0.1400
h_{so}(mm)	15	30	16	24.87
h_{si}(mm)	58	77	60	62.70
θ_{sc}(rad)	0.10	0.20	0.1060	0.1116
θ_{sd}(rad)	0.08	0.18	0.0800	0.0854
h_{pm}(mm)	1	10	4	5.27

age torque and lower torque ripple, which are needed results. The optimization ranges of the machine dimension parameters, their initial values, as well as final optimal values are listed in Table 4. The torque comparison between initial and optimal cases is shown in Figure 11. It can be concluded that the average torque of the DF-DSM can be improved by 24.6% and torque ripple can be reduced by 55.9% with FEA and GA combined optimization.

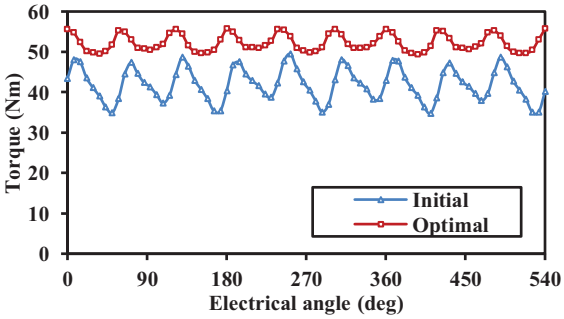

FIGURE 11 Torque in initial and optimal cases

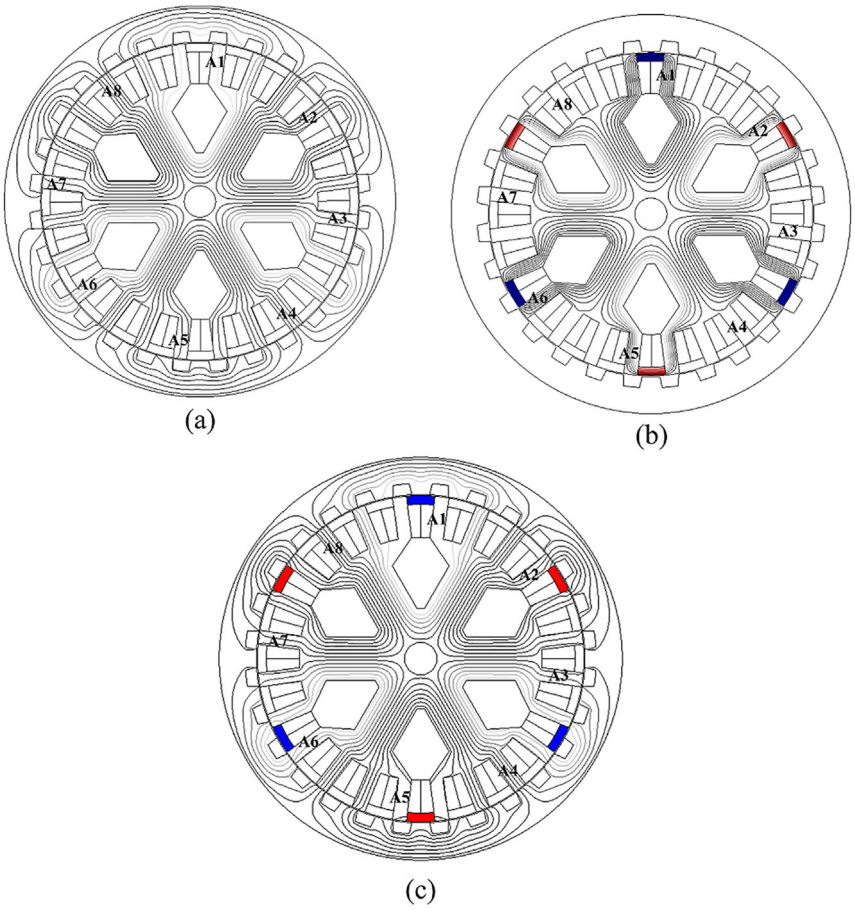

FIGURE 12 No-load flux distribution under different excitation sources. (a) Only 200A idc. (b) Only slot PMs. (C) 200A idc and slot PMs

4 | ELECTROMAGNETIC ANALYSIS OF THE MACHINE

Based on the above optimized results, the 24/28 slot-pole combination optimized DF-DSM is shown in Figure 2, and its electromagnetic performance is further analysed with FEA in this section.

4.1 | No-load performance

Figure 12 shows no-load flux distribution under different excitation sources. It can be noticed that both DC field excitation and slot opening PMs can generate magnetic field. The flux distribution generated by DC field excitation passes through the stator, air gap, and rotor which is showed in Figure 12(a). In the meanwhile, the flux distribution generated by slot PMs does not pass through the rotor or air gap, and only focuses on the stator, which is denoted in Figure 12(b). Figure 12(c) presents the flux distribution with both DC field excitation and slot PMs. Slot PMs can greatly mitigate the stator core saturation caused by DC field excitation.

Figure 13 shows no-load flux linkage of each coil of phase A. It can be seen that the flux linkage of each coil of phase A has almost zero phase shifts no matter with or without slot PMs.

Comparing Figure 13(a) with Figure 13(b), the flux linkage of A3 A4, A7, A8 remains unchanged, while the flux linkage of A1, A2, A5, A6 becomes smaller. From Figure 2, we know that coil A1, A2, A5, A6 are near slot PMs, while coil A3, A4, A7, A8 are relatively far from slot PMs. It can be concluded that the slot PMs have great DC-saturation-relieving effect on the coils near them, while have little effect on the coils far away from them.

Moreover, it can be seen that the left and right side of the flux linkage of each coil of phase A is asymmetric, while the flux linkage of each coil of phase A is not identical due to the different displacements of coil of phase A to the DC excitation coils, no matter with or without slot PMs.

Excited by both dc current and slot PMs, the self-inductance of coil A1 and A2 at rated positive and negative current are shown in Figure 14. It can be observed that their variations are reversed. Similar variations can be found in the coil A3 and A4, A5 and A6, A7 and A8. Therefore, when connecting the coils in series, the resulting variation of self-inductance can be significantly diminished.

Excited by both DC current and slot PMs, the self-inductance of phase A and corresponding mutual inductance between phases A and B are plotted in Figure 15. It can be seen that the mutual inductance is much smaller than the self-inductance due to the nature of concentrated windings.

Comparing Figure 14 with Figure 15, the self-inductance average value of phase A is nearly as large as eight times of

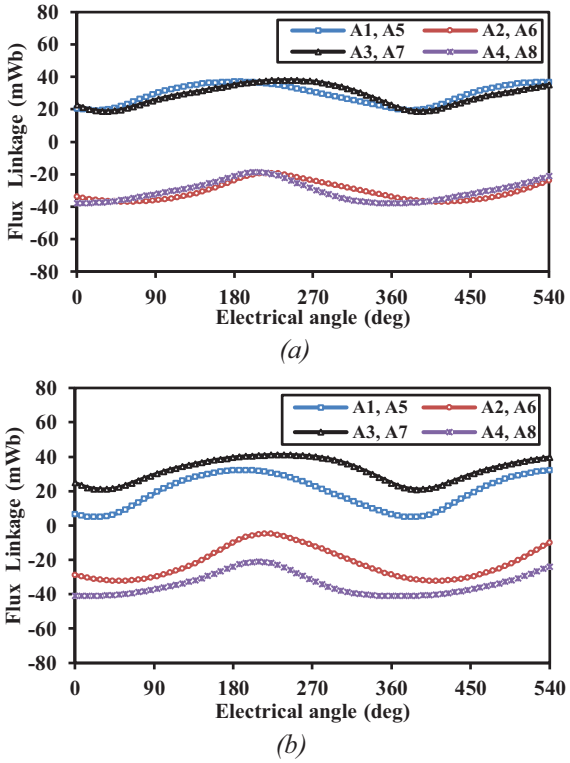

FIGURE 13 No-load flux linkage of each coil of phase A. (a) without slot PMs. (b) with slot PMs

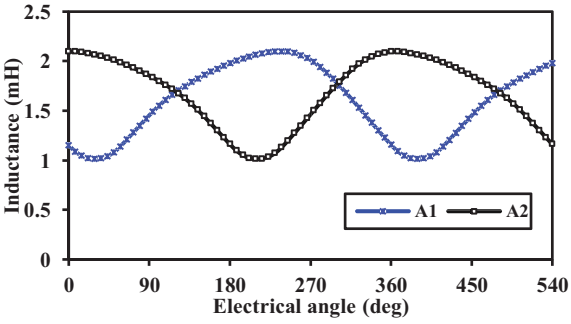

FIGURE 14 No-load self-inductance of coil A1 and A2 excited by both idc and slot PMs

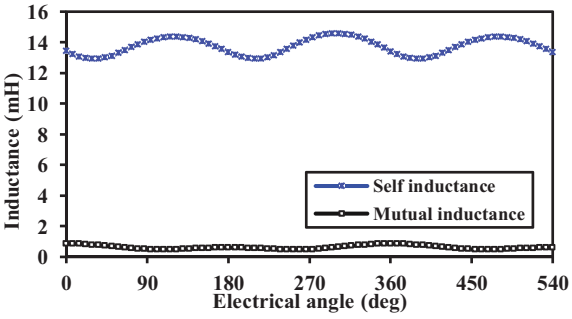

FIGURE 15 No-load self-inductance of phase A and mutual inductance between phase A and B excited by both idc and slot PMs

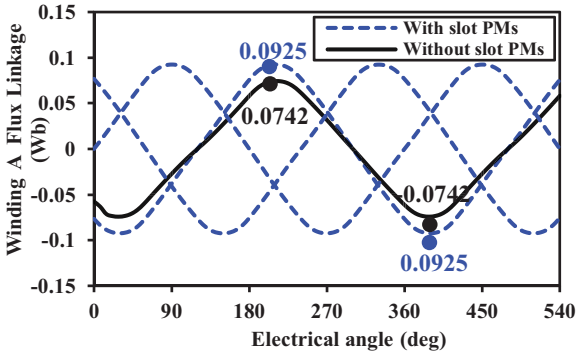

FIGURE 16 No-load flux linkage

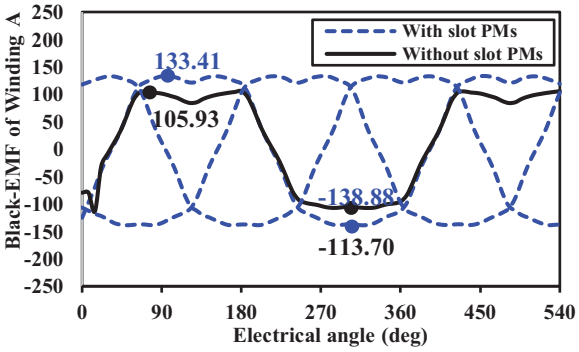

FIGURE 17 No-load back-EMF

self-inductance average value of coil A1. However, the self-inductance peak-to-peak value of phase A is almost the same as the self-inductance peak-to-peak value of coil A1. It is confirmed that the proposed machine offers much smaller variation of self-inductance with special winding connection.

Moreover, the no-load flux linkage is presented in Figure 16. The DC excitation current is given 200 A. Three phase no-load flux linkage with slot PMs is denoted in blue dashed lines. It is obvious that flux linkage realizes three phase symmetry. Compared the blue dashed lines with black solid line, with the introducing of slot PMs, the flux linkage maximum value of phase A increases from 0.0742 to 0.0925 Wb. Meanwhile, the flux linkage minimum value of phase A decreases from −0.0742 to −0.0925 Wb. The flux variation range changes from 0.1482 to 0.185 Wb. Comparing Figure 16 with Figure 13, with the special winding connection, the flux linkage of phase A becomes much more symmetric than that of each coil of phase A.

In addition, since the flux linkage is symmetric with almost liner rise-up and fall-off slops, the resulting back EMF is symmetric and exhibits a wide flat-top range as shown in Figure 17. The blue dashed lines present three phase back-EMF with slot PMs, which achieve three phase symmetry. Compared the blue dashed lines with black solid line, through adopting slot PMs, the black-EMF maximum value of phase A enhances from 105.93 to 133.42 V, and the black-EMF minimum value of phase A reduces from −113.7 to −138.88Nm. This agrees with the previous analysis that the slot PMs can relieve the saturation

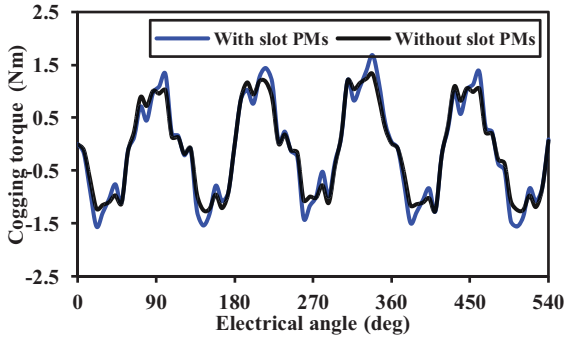

FIGURE 18 No-load cogging toque

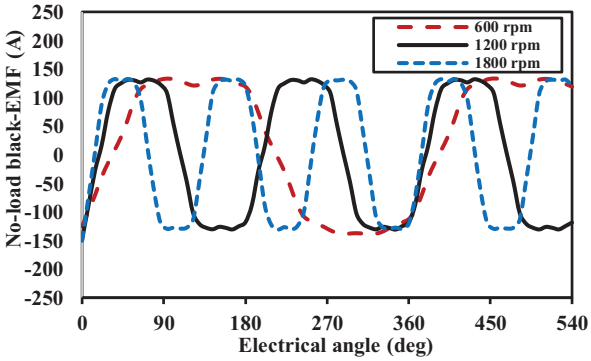

FIGURE 19 No-load back-EMF under different speeds

effect in the stator core, thus more current can be injected to boost the back-EMF under no-load condition.

Figure 18 denotes the cogging torque under no-load condition, which shows that the cogging torque is almost unchanged, no matter with or without slot opening PMs.

Figure 19 shows no-load back-EMF under different operation speeds. It can be found that through regulating the DC field current, the no-load back-EMF can remain the same, which illustrates the variable speed constant voltage wind power generation can be realized.

4.2 | On-load performance

Figure 20 presents the calculated steady torque under on-load condition. The DC excitation current is given 200 A, while the AC excitation current is given 10.78 A with 6 A/mm^2 of rated current density. It can be seen that the average torque with only DC excitation current is 37.36 Nm. In the meantime, the average torque with both DC excitation current and slot PMs is 52.16 Nm, which is enhanced by 39.61% under rated condition. The average torque with only slot PMs indicates that the slot PMs have insignificant contribution to the steady torque.

Figure 21 denotes flux density under rated condition. As marked by the red circles, the saturation effect can be relieved with the introducing of slot PMs.

In addition, power, loss and efficiency of this new machine are assessed with 200 A DC excitation current and 6 A/mm^2

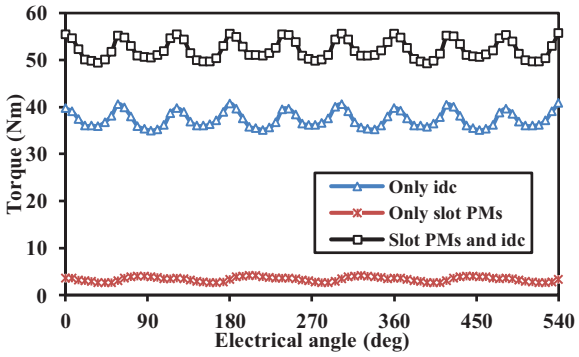

FIGURE 20 Steady torque under rated condition

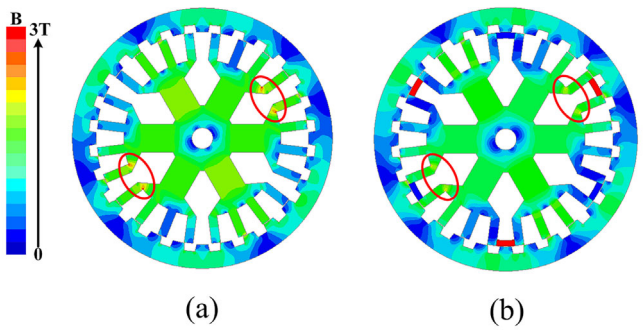

FIGURE 21 Flux density under rated condition. (a) Without slot PMs. (b) With slot PMs

current density of AC excitation current. As shown in Table 5, even though copper loss remains unchanged, while core loss and eddy current loss are higher with the introducing of slot PMs, the rated efficiency increases slightly. It is confirmed that the slot PMs can mitigate the saturation effect of stator core, hence greatly enhance the steady torque, power density, and improve the efficiency.

TABLE 5 Performance comparison of DF-DSM with and without slot PMs

Parameter	Unit	Without slot PMs	With slot PMs
Output power	W	2347.34	3277.15
Input power (Rated power)	W	2662.55	3631.64
Core loss	W	112.55	151.83
Eddy current loss	W	49.86	69.45
Copper loss	W	202.66	202.66
Rated efficiency	/	88.16%	90.24%
Power density	kW/m^3	648.92	905.97

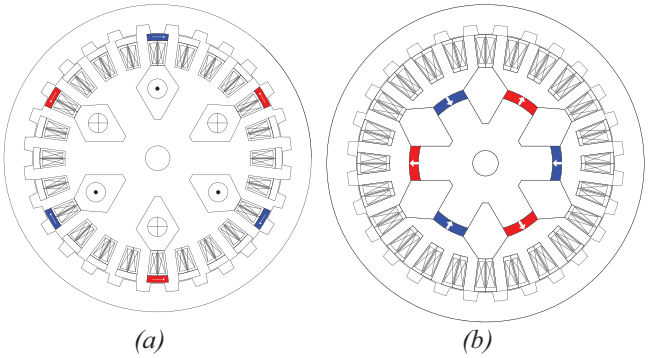

FIGURE 22 (a) Proposed DF-DSM. (b) Conventional DSM

TABLE 6 Performance comparison of proposed DF-DSM and conventional DSM

Parameter	Unit	Proposed machine	Conventional doubly salient machine
Outer radius of stator	mm	120	120
Stack length	mm	80	80
Airgap length	mm	0.6	0.6
Stator slot number	/	24	24
Rotor pole number	/	28	28
Rated torque	Nm	52.16	28.57
Flux regulation capability	/	Good	Bad
Rotor robustness	/	Good	Good
Core loss	W	151.83	149.27
Eddy current loss	W	69.45	61.47
Copper loss	W	202.66	123.28
Output power	W	3277.15	1794.97
Input power	W	3631.64	2067.52
Rated efficiency	/	90.24%	86.82%
Power density	kW/m^3	905.97	496.22

4.3 | Comparative study

A comparison study between proposed DF-DSM and conventional DSM is conducted. The structures of these two machines are shown in Figure 22. The excitation sources of the proposed DF-DSM are DC field winding, AC armature winding, as well as slot PMs, while the excitation sources of the conventional DSM are radial yoke PM and AC armature winding. Their rotors all consist of only iron, which provide mechanical robustness. Two machines share the same design except for different excitation sources and their arrangement.

As shown in Table 6, the outer radius of stator, stack length, airgap length, stator slot number, rotor pole number of these two machines are the same. However, the proposed DF-DSM has higher rated torque, power density, while has better flux regulation capability than the conventional DSM. Comparing to conventional doubly salient machines, the proposed machine has slightly higher core loss and copper loss. However, the power density and efficiency of proposed machine is higher than the conventional doubly salient machine.

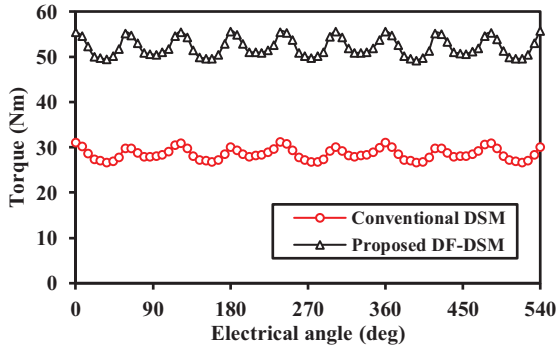

FIGURE 23 Torque comparison between two machines

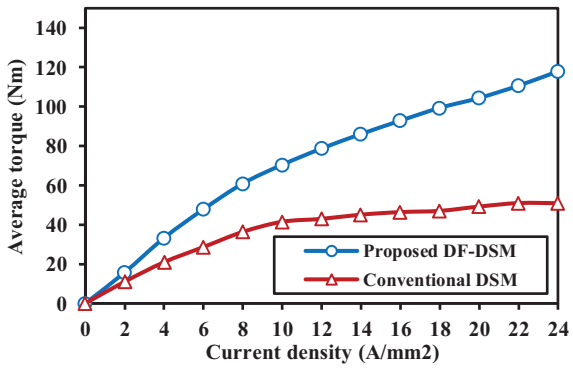

FIGURE 24 Average torque with respect to current density

Figure 23 gives the steady torque of these two machines under rated current density about 6 A/mm^2, which presents excellent torque performance of the proposed DF-DSM. Figure 24 presents the average torque with respect with different current density. When the current density varies from 0 to 24 A/mm^2, the average torque of proposed DF-DSM is always higher than conventional DSM, which illustrates better torque performance of proposed DF-DSM over conventional DSM.

5 | CONCLUSION

In this paper, a novel doubly-fed doubly-salient machine (DF-DSM) with DC-saturation-relieving effect is proposed and verified by FEA. With controllable DC field excitation, the flux can be flexibly controlled, which can extend speed range and capture more wind power. Moreover, with tangentially magnetized PMs mounted on the slot opening, the saturation effect of the stator core can be largely suppressed, hence the steady torque can be enhanced by about 39.61%, power density can be also improved by 39.61%. Last by not least, the comparative study between proposed DF-DSM and conventional DSM is conducted, which illustrates the proposed DF-DSM has better flux regulation capability, and the better overload capability.

In addition, the power density of proposed DF-DSM is significantly higher than the conventional DSM. Although the proposed machine is designed for low power application, it is also suitable for high power application with main excitation source of DC field excitation.

ACKNOWLEDGMENTS

This work was supported by the National Natural Science Foundation of China under Project 52077187 and in part by the Research Grant Council of the Hong Kong Government under Project PolyU 152143/18E and PolyU 152109/20E.

ORCID

Jifu Jiang https://orcid.org/0000-0002-3846-0139

REFERENCES

1. Zinger, D., Mujadi, E.: Annualized wind energy improvement using variable speed. IEEE Trans. Ind. Appl. 33(6), 1444–1447 (1997).
2. Soder, L., Ackermann, T.: Wind energy technology and current status: A review. Renewable Sustainable Energy Rev. 4, 315–374 (2000)
3. Soderlund, L., Eriksson, J.-T., Salonen, J.: A permanent-magnet generator for wind power applications. IEEE Trans. Magn. 32(4), 2389–2392 (1996).
4. Bhowmik, S., Spee, R., Enslin, J.H.R.: Permanence optimization for doubly fed wind power generation systems. IEEE Trans. Ind. Appl. 35(4), 949–958 (1999).
5. Zhu, X., et al.: Overview of flux-modulation machines based on flux-modulation principle: Topology, theory, and development prospects. IEEE Trans. Transp. Electrif. 6(2), 612–624 (2020).
6. Burton, T., et al.: Wind Energy Handbook. John Wiley & Sons Ltd, Chichester, UK (2001)
7. Wei, J., Zhou, B., Cheng, F.-S.: A new three-phase doubly salient electrical magnet generator for direct-driven wind power generation. In: 2008 International Conference on Electrical Machines and Systems, Wuhan, pp. 4250–4252 (2008)
8. Zhang, J., Cheng, M., Feng, X.: Design and comparison of wind power permanent magnet generator with doubly salient structure and full pitched windings. In: 2011 4th International Conference on Electric Utility Deregulation and Restructuring and Power Technologies (DRPT), Weihai, Sahngdong, pp. 1329–1334 (2001)
9. Cheng, M., Chau, K.T., Chan, C.C.: Design and analysis of a new doubly salient permanent magnet motor. IEEE Trans. Ind. Appl. 31(5), 1069–1078 (1995)
10. Niu, S., et al.: A novel axial-flux-complementary doubly salient machine with boosted PM utilization for cost-effective derect-drive applications. IEEE Access 7, 145970–145977.
11. Sheng, T., Niu, S.: A novel design method for the electrical mahines with biased DC excitation fluxLinkage. IEEE Trans. Magn. 53(6), 1–4 (2017).
12. Lin, M., Hao, L.: A novel axial field flux-switching permanent magnet wind power generator. IEEE Trans. Magn. 47(10), 4457–4460 (2011).
13. Fan, Y., Chau, K.T., Niu, S.: Development of a new brushless doubly fed doubly salient machine for wind power generation. IEEE Trans. Magn. 42(10), 3455–3457 (2006).
14. Liu, X., Zhu, Z.Q.: Comparative study of novel variable flux reluctance machines with doubly fed doubly salient machines. IEEE Trans. Magn. 49(7), 3838–3841 (2013).
15. Kong, X.: Extreme learning machine based phase angle control for stator-doubly-fed doubly salient motor for electric vehicles. In: 2008 IEEE Vehicle Power and Propulsion Conference, Harbin, China, pp. 1–5 (2008)
16. Zhao, X., et al.: A new relieving-DC-saturation hybrid excitation vernier machine for HEV starter generator application. IEEE Trans. Ind. Electron. 67(8), 6342–6353 (2020).
17. Zhao, X., Niu, S., Fu, W.: Sensitivity analysis and design optimization of a new hybrid-excited dual-PM generator with relieving-DC-saturation structure for stand-alone windpower generation. IEEE Trans. Magn. 56(1), 1–5 (2020)
18. Afinowi, I.A.A., et al.: Hybrid-excited doubly salient synchronous machine with permanent magnets between adjacent salient stator Poles. IEEE Trans. Magn. 51(10), 1–9 (2015).
19. Afinowi, I.A.A., Zhu, Z.Q., Guan, Y.: A novel brushless AC doubly salient stator slot permanent magnet machine. IEEE Trans. Energy Convers. 31(1), 283–292 (2016).
20. Zhu, Z.Q., et al.: Hybrid excited stator slot PM machines with overlapping windings. In: 2018 XIII International Conference on Electrical Machines (ICEM), Alexandroupoli, pp. 2185–2191 (2018)
21. Zhao, X., et al.: Design of a new relieving-DC-saturation hybrid reluctance machine for fault-tolerant in-wheel direct drive. IEEE Trans. Ind. Electron. 67(11), 9571–9581 (2020).
22. Zhao, X., Niu, S., Fu, W.: A new modular relieving-DC-saturation vernier reluctance machine excited by zero-sequence current for electric vehicle. IEEE Trans. Magn. 55(7), 1–5 (2019)
23. Shen, Y., Zeng, Z., Lu, Q.: Investigation of a modular linear doubly salient machine with dual-PM in primary yoke and slot openings. IEEE Trans. Magn. 55(6), 1–6 (2019).
24. Shen, Y., Lu, Q.: Design and analysis of linear hybrid-excited slot permanent magnet machines. IEEE Trans. Magn. 54(11), 1–6 (2018).

How to cite this article: Jiang, J., et al.: A novel doubly-fed doubly-salient machine with DC-saturation-relieving structure for wind power generation. IET Renew. Power Gener. 15, 2042–2051 (2021). https://doi.org/10.1049/rpg2.12225